

## Probabilistic-based damage identification based on error functions with an autofocusing feature

Rahim Gorgin<sup>1</sup>, Yunlong Ma<sup>2</sup>, Zhanjun Wu<sup>\*1</sup>, Dongyue Gao<sup>1</sup> and Yishou Wang<sup>1</sup>

<sup>1</sup>State Key Laboratory of Structural Analysis for Industry Equipments, School of Aeronautics and Astronautics, Dalian University of Technology, Dalian 116024, Liaoning, China  
<sup>2</sup>Beijing Aerospace System Engineering Institute, Beijing, China

(Received May 9, 2014, Revised November 8, 2014, Accepted November 18, 2014)

**Abstract.** This study presents probabilistic-based damage identification technique for highlighting damage in metallic structures. This technique utilizes distributed piezoelectric transducers to generate and monitor the ultrasonic Lamb wave with narrowband frequency. Diagnostic signals were used to define the scatter signals of different paths. The energy of scatter signals till different times were calculated by taking root mean square of the scatter signals. For each pair of parallel paths an error function based on the energy of scatter signals is introduced. The resultant error function then is used to estimate the probability of the presence of damage in the monitoring area. The presented method with an autofocusing feature is applied to aluminum plates for method verification. The results identified using both simulation and experimental Lamb wave signals at different central frequencies agreed well with the actual situations, demonstrating the potential of the presented algorithm for identification of damage in metallic structures. An obvious merit of the presented technique is that in addition to damages located inside the region between transducers; those who are outside this region can also be monitored without any interpretation of signals. This novelty qualifies this method for online structural health monitoring.

**Keywords:** damage detection; Lamb wave; probabilistic-based algorithm; scatter signal; error function

### 1. Introduction

To ensure structural integrity and hence maintain safety during service, active structural health monitoring (SHM) techniques have found important roles throughout the aerospace, mechanical, and civil engineering communities. Traditional non-destructive evaluation (NDE) techniques (e.g., X-ray imaging, ultrasonic scans, infrared thermography, acoustic wave propagation, and eddy current) are somehow difficult to implement, and some of them are impractical in many cases such as in-service aircraft testing and in situ space structures. In contrast, SHM is an emerging technology with intelligent algorithms to interrogate the 'health' condition of structures in real time or whenever necessary (Ihn and Chang 2008).

Toward this topic, Lamb waves, ultrasonic guided waves that propagate inside thin-wall plates and shallow shells, have been increasingly employed to develop various SHM techniques (Ihn and Chang 2008, Kundu *et al.* 2009, Ihn and Chang 2004, Wang and Yuan 2005, Wu and Chang 2009,

---

\*Corresponding author, Professor, E-mail: wuzhj@dlut.edu.cn

Sohn and Lee 2010, Wang *et al.* 2003, Wang *et al.* 2004, Lin and Giurgiutiu 2006, Hu *et al.* 2008). As Lamb waves travel long distances in structure and can be applied with conformable piezoelectric (PZT) actuators/sensors that require little power, they are suitable for structural health monitoring (Sohn *et al.* 2004). Basically, when an elastic wave travels through a region where there is a change in material properties, scattering occurs in all directions. SHM methods utilize the distributed actuators/sensors, permanently attached to the structure, to generate the elastic wave and measure the arriving waves at sensors. Accurate interpretation of captured Lamb wave signals is critical for the Lamb wave based damage identification algorithms.

Time-of-flight can be a straightforward parameter for triangulating damage in some cases (Su *et al.* 2006). However, it is quite difficult to extract this kind of damage-sensitive feature due to the complex mechanisms of Lamb wave propagation in structures, even with a large number of sophisticated signal processing techniques. To tackle these deficiencies tremendous efforts have been directed toward identifying structural damage quantitatively through appropriate inverse algorithms, represented by artificial neural networks (Su and Ye 2004, Ye *et al.* 2006), genetic algorithms (Coverley and Staszewski 2003, Ling *et al.* 2005), and support vector machines (Worden and Lane 2001, Park *et al.* 2006).

Another promising alternative is probabilistic-based techniques (Wang *et al.* 2010, Zhou *et al.* 2011). These techniques can efficiently minimize the dependence on subjective interpretation of signals. Nevertheless, conventional probabilistic-based methods are just able to highlight damages located inside the region between transducers.

This study focuses on the estimation of the probability of the presence of damage in the monitoring area by using some sets of transducers. To avoid the need for direct interpretation of overlaid and dispersed Lamb wave components, a probabilistic based damage detection algorithm is employed. To achieve this, changes in Lamb wave signals between the present state (with damage) and the baseline (without damage) is measured. Subsequently, the energy of scatter signals till different times were calculated by taking root mean square of the scatter signals. For each pair of parallel paths an error function based on the energy of scatter signals is introduced. The resultant error function then is used to construct the probability image in the monitoring area. Both finite element analysis and experimental evaluations at different central frequencies are presented in this study, demonstrating the potential of such a probabilistic based algorithm for identifying damage in metallic structures. An obvious merit of the present technique is that in addition to damages located inside the region between transducers; those who are outside this region can also be monitored without any interpretation of signals.

## 2. Methodology

In this study, a probabilistic-based method is proposed to identify damage location by analyzing the scattered waves induced at structural flaws. When an elastic wave, such as Lamb wave, is generated from a transmitter and travels through a region where there is a change in material properties due to damage, wave scattering occurs in all directions. The damage can be considered as a wave scattering source and measured scattered waves at sensors will be utilized to investigate the damage.

Fig. 1 illustrates the approach. For a given network of 4 Sensors, the response of the healthy structure,  $b_i(t)$  is collected for parallel paths. Furthermore, assuming damage has occurred in the structure, the response of the damaged structure,  $d_i(t)$  is also collected for such paths.

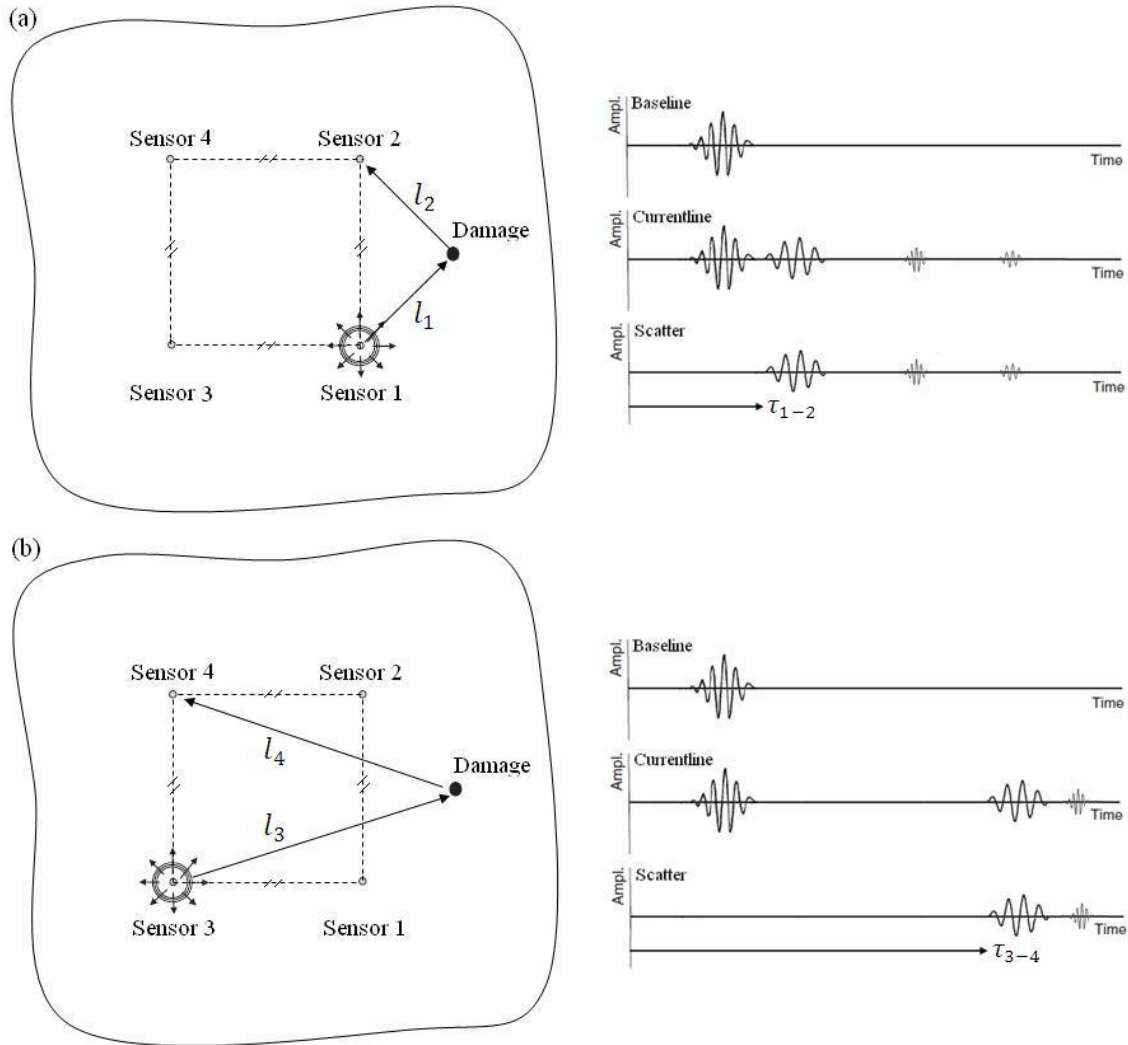


Fig. 1 Diagnostic approach: (a) Path 1-2 and (b) Path 3-4

A signal-processing scheme based on short time Fourier transform (STFT) which are particularly effective for analysis and visualization of lamb wave signals, is utilized to extract useful diagnostic information. The STFT of a raw signal  $f(t)$  is defined as

$$f(\omega, t) = \frac{1}{2\pi} \int_{-\infty}^{\infty} e^{-i\omega\tau} f(\tau)h(\tau - t)d\tau \tag{1}$$

Since the window function,  $h(t)$ , has a short time duration, by moving  $h(t)$  with Fourier integrals, the signal's local frequency properties evolving over time can be revealed.

The scattered response  $s_i(\omega_0, t) = d_i(\omega_0, t) - b_i(\omega_0, t)$  at driving frequency  $\omega = \omega_0$ , is contained the scattered waves coming from the damage and structure boundaries.

As illustrated in Figs. 1(a) and 1(b), the time of flights (TOF)  $\tau_{1-2}$ , of the scattered wave

should correspond to the wave travel time from Sensor 1 to the damage and then from the damage to Sensor 2 and  $\tau_{3-4}$ , is the wave travel time from Sensor 3 to the damage and then from the damage to Sensor 4 such that

$$l_1 + l_2 = c\tau_{1-2} \quad (2)$$

$$l_3 + l_4 = c\tau_{3-4} \quad (3)$$

Where,  $l_1$ ,  $l_2$ ,  $l_3$ , and  $l_4$  are the linear distance between the damage and respectively with Sensors 1, 2, 3 and 4.  $c$ , is the wave speed.

Assuming the velocity is constant, the locus of the possible damage location is an ellipse with Sensor 1 and Sensor 2 as the foci. In order to find the exact location of the scatter source or damage, other ellipses generated from other paths (e.g., path 3-4) need to be used. This method was previously proposed and its feasibility was demonstrated by generating a crude digital image of added mass on a flat aluminum plate using distributed piezoelectric actuator/sensors (Wang *et al.* 2003, Wang *et al.* 2004).

However, it is quite difficult to extract accurate time of flight due to the complex mechanism of lamb wave propagation in engineering structures, even with a large number of sophisticated signal processing algorithms. To overcome this difficulty, a probabilistic based algorithm is presented.

Assuming the wave speed  $c$  is constant and the same for all paths, then based on Eqs. (2) - (3) it can be written

$$\frac{l_1+l_2}{l_4+l_3} = \frac{\tau_{1-2}}{\tau_{3-4}} \quad (4)$$

For both paths, the energy of the scattered signal till different times can be computed by taking the root mean square (RMS) of scattered response as follows

$$RMS(t_i) = \sqrt{\frac{\sum_{k=0}^i s(\omega_0, t_k)^2}{Z}} \quad (5)$$

Here,  $RMS(t_i)$  is the energy of the scatter signal till ( $t = t_i$ ),  $s(\omega_0, t_k)$  is the amplitude of the scatter signal at ( $t = t_k$ , and  $\omega = \omega_0$ ), and  $Z$  is the number of data points.

As illustrated in Fig. 2, the energy of the scatter signals of paths 1-2 and 3-4 respectively, at times  $\tau_{1-2}$  and  $\tau_{3-4}$  starts to increase.

Based on the distance of each path to the damage and also to the structure boundaries, the scatter signal energy at different times reach to a definite value. Paths closer to the damage, receive the scatter waves earlier so these paths earlier reach to a definite value of the scatter signal energy. Paths with the same distance to the damage and to the structure boundaries receive scatter waves at the same time so at the same time they reach to a definite value of the scatter signal energy.

Although the times which the energy of the scatter signal of paths 1-2 and 3-4 reach to a definite value is different from their time of flights, still as can be recognized from Fig. 2, the ratio of these times is close to the ratio of their time of flights such that

$$\frac{\tau_{1-2}}{\tau_{3-4}} \cong \frac{t_{1-2}(RMS_i)}{t_{3-4}(RMS_i)} \quad 0 < RMS_i \leq \beta_1 \quad (6)$$

Where,  $t_{1-2}(RMS_i)$  and  $t_{3-4}(RMS_i)$  are the times when the scatter signal energy of paths 1-2 and 3-4 reach to the value,  $RMS_i$ , respectively. As shown in Fig. 2,  $\beta_1$ , denotes a threshold level for the scatter signal energy to be used in Eq. (6).

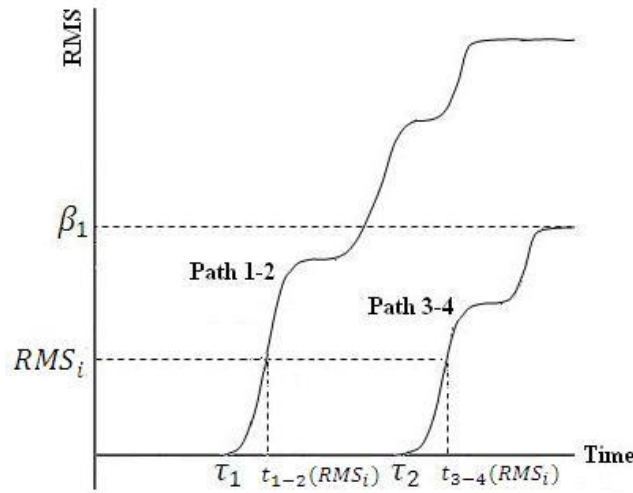


Fig. 2 The growth of scatter signals energy

Because, for the scatter signal energy values more than  $\beta_1$ ,  $t_{3-4}(RMS_i)$  cannot be defined. Substituting Eq. (6) into Eq. (4) leads to

$$\frac{l_1+l_2}{l_4+l_3} \cong \frac{t_{1-2}(RMS_i)}{t_{3-4}(RMS_i)} \quad 0 < RMS_i \leq \beta_1 \tag{7}$$

Since the wave speed is not constant and is different for all paths besides the differences between  $\frac{t_{1-2}(RMS_i)}{t_{3-4}(RMS_i)}$  and  $\frac{\tau_{1-2}}{\tau_{3-4}}$ , an error function is introduced based on Eq. (6) as follow

$$\epsilon_1 = \frac{\sum_{i=0}^{\beta_1} \left| (l_1+l_2) - \left[ \frac{t_{1-2}(RMS_i)}{t_{3-4}(RMS_i)} \times (l_3+l_4) \right] \right|}{N} \tag{8}$$

Here,  $N = \beta_1/\Delta s$ , is the number of samples according to the sampling period ( $\Delta s$ ) of the scattered energy. For each pair of parallel paths an error function can be introduced. For instance, in this set of transducers another error function can be introduced based on paths 1-3 and 2-4 such that:

$$\epsilon_2 = \frac{\sum_{i=0}^{\beta_2} \left| (l_1+l_3) - \left[ \frac{t_{1-3}(RMS_i)}{t_{2-4}(RMS_i)} \times (l_2+l_4) \right] \right|}{N} \tag{9}$$

Here,  $\beta_2$  is the threshold level for the scatter signal energy of paths 1-3 and 2-4. Using other sets of transducers in different regions of plate gives more error functions and enhances the reliability of the presented algorithm. Finally, the resultant error function can be determined as follows

$$\epsilon = \sqrt{\epsilon_1^2 + \epsilon_2^2 + \dots} \tag{10}$$

The resultant error function is used to estimate the probability of the presence of damage in the structure. To achieve this, the monitoring area is meshed into uniformly distributed grids and the resultant error function is determined for each grid. Regions with the minimum values of the resultant error function show the most probable location of damage.

### 3. Finite element analysis procedures

Finite element analysis were conducted to investigate the generation and acquisition of lamb wave signals in an aluminum plate ( $49\text{ cm} \times 49\text{ cm} \times 3\text{ cm}$ ) and to identify a hole ( $\varnothing 2\text{ cm}$ ) using the probabilistic-based damage identification algorithm. The aluminum plate, set up with eight surface-mounted piezoelectric discs of  $6.6\text{ mm}$  in diameter and  $0.24\text{ mm}$  in thickness, was modeled using MSC.Patran<sup>®</sup>. A circular epoxy layer of  $6.6\text{ mm}$  in diameter and  $0.02\text{ mm}$  in thickness is placed between each piezoelectric disc and the plate. The mechanical properties of the plate and epoxy layer are listed in Table 1.

The specimen geometry and configuration of sensor sets are illustrated in Fig. 3.

A coordinate system (Fig. 3) was employed in the monitoring area spanned by the horizontal,  $x$  and vertical,  $y$ , axes, where the origin was at the corner of the plate. The coordinate of the central location of the hole were ( $x=18\text{ cm}$ ,  $y=31\text{ cm}$ ). Free boundary conditions were employed along four edges.

The plate was finely meshed using 8-node 3-dimensional brick elements and PZT transducers are modeled using piezoelectric element. Piezoelectric elements properties can be found in Table 2.

Table 1 Mechanical properties of aluminum plate and epoxy layer

	Young's modulus $E$ (GPa)	Poisson's ratio $\nu$	Density $\rho$ ( $\text{kg}/\text{m}^3$ )
Plate	70	0.33	2700
Epoxy layer	14	0.31	1400

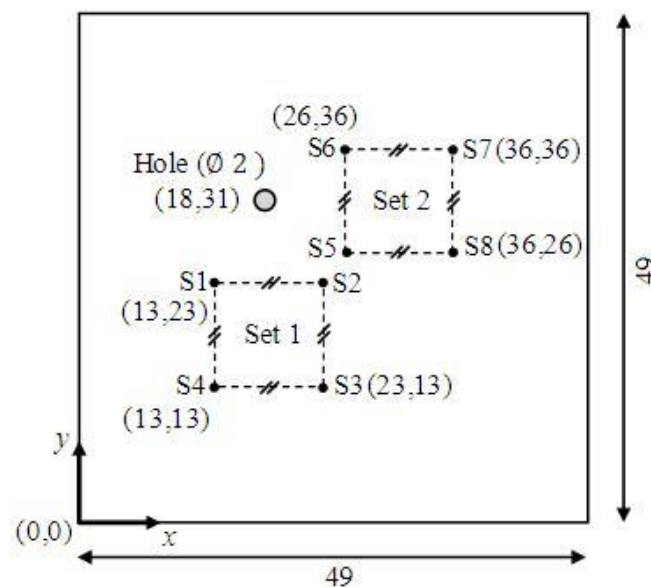


Fig. 3 Schematic diagram of aluminum plate with a Hole for FEM computation (dimensions in cm)

Table 2 Material properties of PZT transducer

Product name	APC 851
Geometry (mm)	$\varnothing = 6.6, \quad h_{\text{PZT}} = 0.24$
Density (g/cm <sup>3</sup> )	7.6
Electromechanical coupling factor $k_p$	0.71
Voltage constant $g_{33}$ (Vm/N)	$24.8 \times 10^{-3}$
Charge constant $d_{33}$ (m/V)	$400 \times 10^{-12}$
Relative dielectric constant $K^T$	1950
Frequency constant $N_T$ Hz. m	2040
Elastic constant E GPa	63

The dynamic simulation of lamb wave activation and propagation was accomplished employing ABAQUS/Implicit<sup>®</sup> code. The element size in the plane was set as 2 mm and six layers were modeled in the thickness direction. A hole was simulated by removing the equivalent elements.

A 5-cycle sinusoidal toneburst enclosed in a Hanning window at a central frequency of 150 KHz was imposed as potential differences between the upper and lower surface of the piezoelectric elements of the actuator and acquired at a sampling rate of 48 MHz in a time period of 167  $\mu$ s, consistent with the configuration for subsequent experiment.

#### 4. Experimental set up

An aluminum plate with the same geometry, mechanical properties, and boundary conditions as in finite element analysis is experimentally evaluated. The hole is introduced by a Drilling machine. The hole was exactly located at the same position as the finite element analysis. Eight piezoelectric discs (APC 851) with properties given in Table 2, were surface-mounted at the same positions as the finite element analysis.

Piezoelectric discs are attached to the plate using an epoxy adhesive with properties given in Table 1. Piezoelectric discs acted as both actuators and sensors with the aid of a two-way switch. Generation and acquisition of lamb waves were fulfilled using Scan Genie machine.

In accordance with the simulation, a 5-cycle sinusoidal toneburst enclosed in a Hanning window at a central frequency of 150 kHz was generated and acquired at a sampling rate of 48 MHz. Sampled signals were transmitted into the central processing unit for further analysis.

All the diagnosis control and signal analysis were performed using central processing unit. Configuration of proposed diagnosis system is illustrated in Fig. 4.

Different central frequencies (200 kHz and 250 kHz) were also used to validate the robustness of the probabilistic-based method.

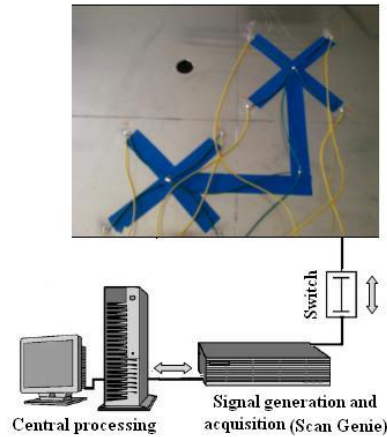


Fig. 4 Configuration of proposed diagnosis system

## 5. Results and discussion

### 5.1 Error functions

On The response of the intact and damaged plate using FEM analysis is collected for parallel paths of each set. The scattered or difference response of different paths are then specified and those of set 1 are illustrated in Fig. 5. The scatter signals contain scatter waves directly coming from damage and some reflection of the scatter wave from plate boundaries. Using Eq. (3), the RMS values of the scattered signals till different times are determined. Fig. 6 demonstrate the RMS values of scattered signals against time for different paths of both sets. The RMS values are normalized.

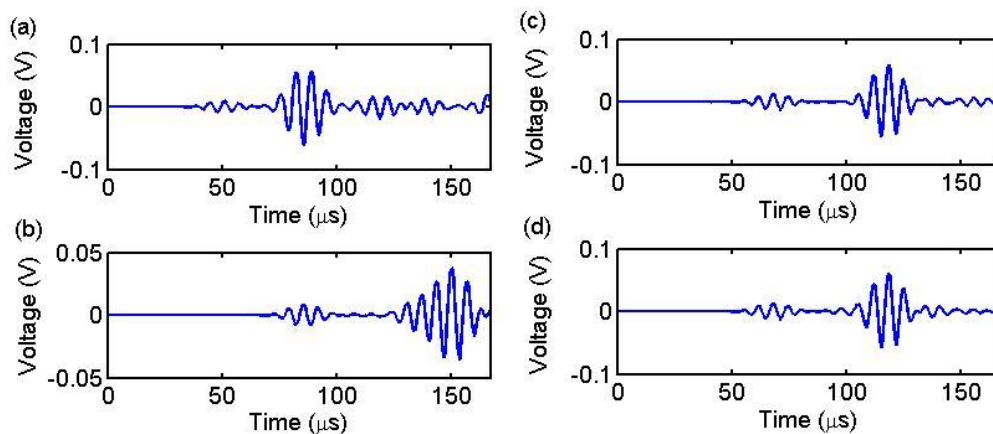


Fig. 5 Simulation scatter signals from sensing paths: (a) Path 1-2; (b) Path 3-4; (c) Path 1-4; (d) Path 2-3

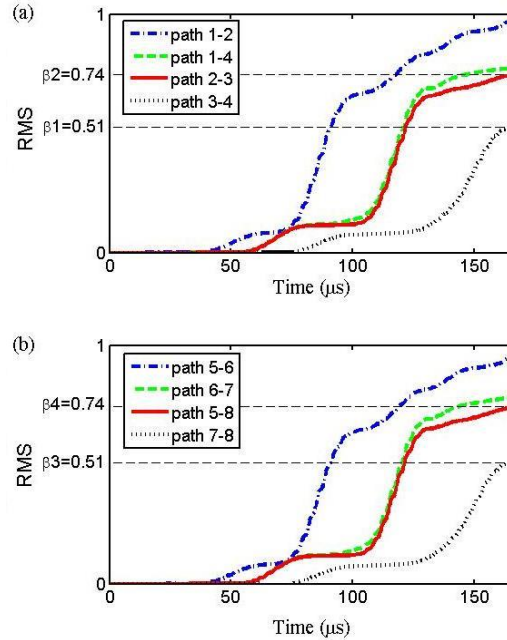


Fig. 6 The energy of simulation scatter signals till different times: (a) Set 1 and (b) Set 2

Regarding to Fig. 6, paths with the same distance to the damage and also to the structure boundaries, have the same values of RMS till different time (e.g., compare paths 1-2 with 5-6). This emanated from receiving all scatter waves at the same times. Those paths with the same distance to the damage but with different distance to the structure boundaries have the same values of RMS until they just receive the scatter wave coming directly from damage, but after that they have different RMS values due to their different reflected scatter waves from structure boundaries (e.g., compare paths 1-4 with 2-3). And finally, paths closer to the damage receive the scatter wave which coming directly from damage earlier than other paths so the RMS values of these paths till different times are more (e.g., compare paths 1-2 with 3-4).

As shown in Figs. 6(a) and 6(b), for each pairs of parallel paths, the threshold level is determined ( $\beta_1 = 0.51$  for paths 1-2 and 3-4;  $\beta_2 = 0.74$  for paths 1-3 and 2-4;  $\beta_3 = 0.51$  for paths 5-6 and 7-8;  $\beta_4 = 0.74$  for paths 5-8 and 6-7). Then a sampling period ( $\Delta s = 0.01$ ) is considered to choose different values of RMS values (RMS=0.01, 0.02, 0.03,...,0.51 for paths 1-2 and 3-4; RMS=0.01, 0.02, 0.03,...,0.74 for paths 1-3 and 2-4; RMS=0.01, 0.02, 0.03,...,0.51 for paths 5-6 and 7-8; RMS=0.01, 0.02, 0.03,...,0.74 for paths 5-8 and 6-7). Subsequently, for each pair of paths, the times that both paths reach to the same RMS value are defined and by Eq. (8) different error functions ( $\epsilon_1$  based on paths 1-2 and 3-4;  $\epsilon_2$  based on paths 1-3 and 2-4;  $\epsilon_3$  based on paths 5-6 and 7-8;  $\epsilon_4$  based on paths 5-8 and 6-7) are specified.

The  $490 \times 490$  uniformly distributed grids (with an interspatial distance of 1.0 mm) were utilized to show error function values at different regions of the monitoring area. Fig. 7 shows the values of different error functions at different regions of the plate. The error function values are normalized.

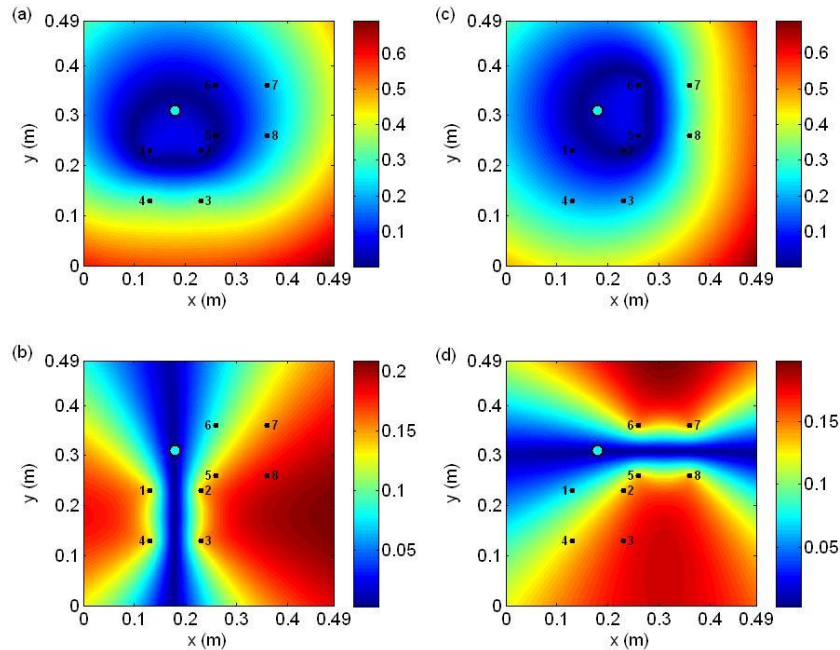


Fig. 7 The simulation error function values: (a)  $\epsilon_1$ ; (b)  $\epsilon_2$ ; (c)  $\epsilon_3$ ; (d)  $\epsilon_4$

According to Fig. 7, for each error function a region with the minimum values is highlighted on the plate. These regions show the probable locations of damage in plate. As shown in Fig. 6, the differences between the ratios,  $\frac{t_{1-2}(RMS_i)}{t_{3-4}(RMS_i)}$  and  $\frac{\tau_{1-2}}{\tau_{3-4}}$ , is more than the differences between the ratios,  $\frac{t_{1-3}(RMS_i)}{t_{2-4}(RMS_i)}$  and  $\frac{\tau_{1-3}}{\tau_{2-4}}$ , therefore regarding to Figs. 7(a) and 7(b), the regions with minimum values of error function  $\epsilon_1$  go through the region near the location of the simulated Hole while the regions with minimum values of error function  $\epsilon_2$  directly passes the region of the simulated Hole. This condition also applies to error functions  $\epsilon_3$  and  $\epsilon_4$  as can be seen in Figs. 7(c) - 7(d).

Experimental process followed the same as finite element procedure. The response of the intact and damaged plate is collected for parallel paths of each set and based on them the scattered or difference response of those paths are specified. In experimentally situations signals are usually accompanied with some noise. Therefore some wrong scatter waves will appear in scatter signals.

Hence, in order to eliminate these wrong scatter waves, only the scatter waves with amplitude above 20% of the maximum amplitude of the scatter signal are retained and the remaining scatter waves, related to noise, are discarded. Fig. 8 illustrates the RMS values of the scattered signals till different times.

The RMS values are normalized. Comparing experimental scatter signal energy of different paths with simulation results shows that the experimental scatter signal energy of path 3-4 is wrong.

This emanated from determining wrong baseline or current line signal of this path. However, obtaining wrong signals which may have different sources of error are inevitable in experimentally conditions.

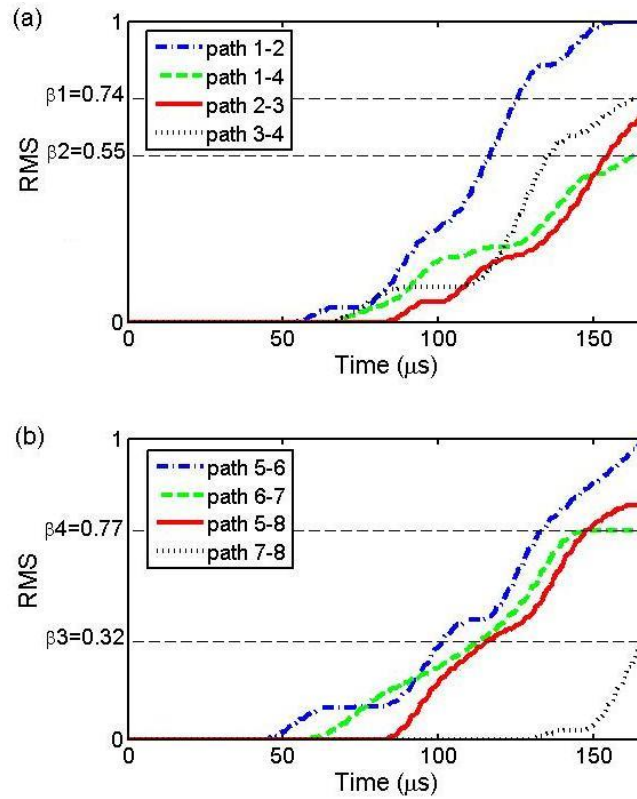


Fig. 8 The energy of experimental scatter signals till different times: (a) Set 1; (b) Set 2

All error functions based on experimental results are determined and shown in Fig. 9. As it is obvious in Fig. 9(a), since the scatter signal energy of path 3-4 was wrong, the error function  $\epsilon_1$  is also wrong and the region with the minimum values of error function  $\epsilon_1$  is far from the location of real Hole. Nevertheless, based on Figs. 9(b)-9(d), error functions,  $\epsilon_2$ ,  $\epsilon_3$  and  $\epsilon_4$  are completely matched with simulation results. These error functions will be used to identify the location of damage.

### 5.2 Damage identification

The  $490 \times 490$  uniformly distributed grids (with an interspatial distance of 1.0 mm) were utilized to construct the image of the probability of the presence of damage in the monitoring area. For each grid, the resultant error function is determined using simulation and experimental error functions. Grids with minimum values of the resultant error function indicate probable location of damage. Fig. 10 illustrates the probability of the presence of damage using simulation and experimental signals at 150 KHz.

The location of actual hole is marked by 'o', while the central location of identified Hole (the grid with the minimum value of the resultant error function) is marked by 'x'. The probability values were normalized.

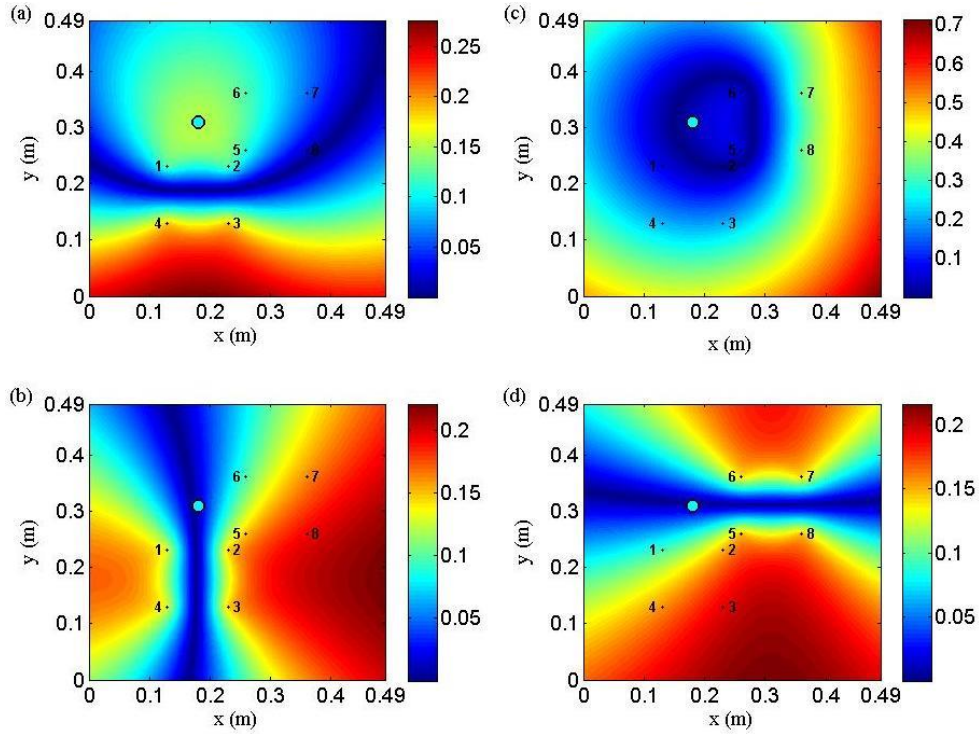


Fig. 9 The experimental error function values: (a)  $\epsilon_1$ ; (b)  $\epsilon_2$ ; (c)  $\epsilon_3$ ; (d)  $\epsilon_4$

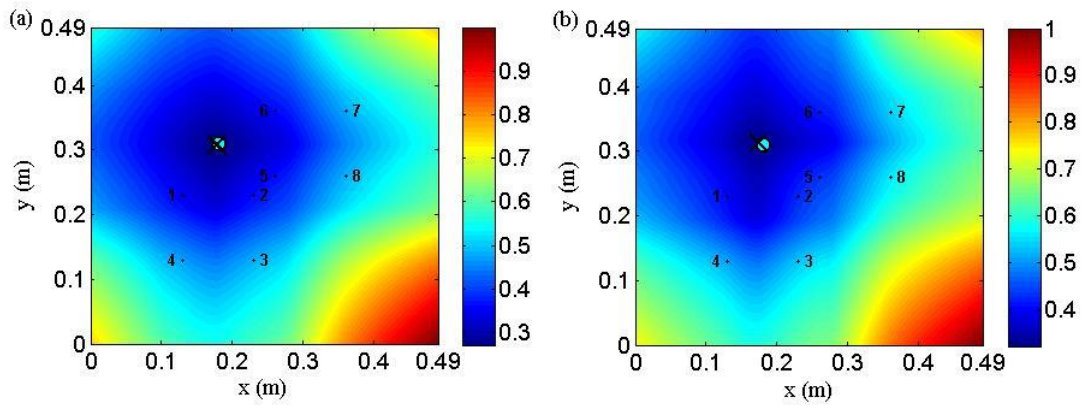


Fig. 10 Probability of the presence of Hole (150 KHz): (a) using simulation signals and (b) using experimental signals

As shown in Fig. 10, the location of simulated and actual Hole can be identified very clearly from the resultant error functions. It should be noted that although one of the experimental error functions was totally wrong, still the resultant error function can display the location of the Hole

clearly. Hence, the novelty of the probabilistic-based algorithm used in the present work is that even if the response of the intact or damaged structure in one or some of the paths defined incorrectly due to different sources of error, still the total results can illuminate the location of damage clearly. It is obvious that using more error functions will enhance the reliability of the proposed method. For example as shown in Fig. 11, the experimental resultant error function defined by using 6 error functions will highlight the exact location of damage.

To validate the robustness of the probabilistic-based algorithm, different central frequencies were used in experiment. The probability images using the proposed experimental signals at 200 and 250 KHz are demonstrated in Fig. 12.

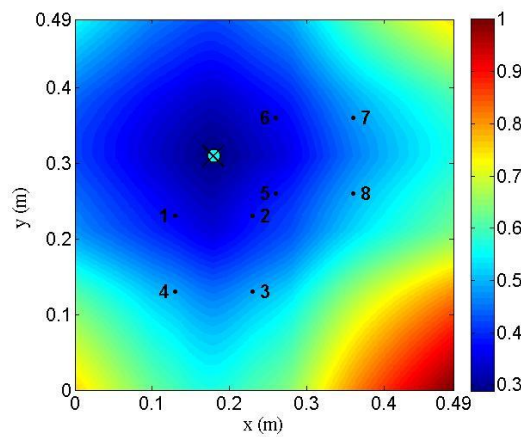


Fig. 11 Probability of the presence of Hole (150 KHz) defined by 6 error functions using experimental signals

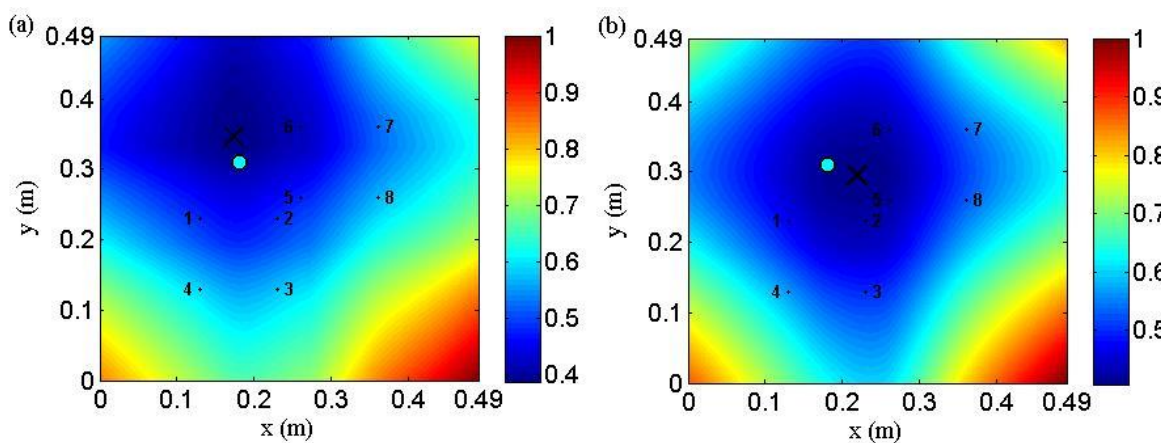


Fig. 12 Probability of the presence of Hole using experimental signals: (a) 200 KHz; (b) 250 KHz

The central location of identified Hole at different central frequencies is near the location of the actual situation and we can still identify the location of the Hole within the acceptable accuracy. The damage scatter signal can be separated into two parts in time domain; scatter wave directly come from damage and reflections of damage scatter wave from structure boundaries. In presented approach, the ratio of times which scatter signal energy reach to definite value is an appropriate substitution for the ratio of times of flight (Eq. (6)), only in the first part of the scatter signal which the sensor capture the scatter wave directly come from the damage. In the second part of scatter signal which includes damage scatter reflections from structure boundaries, this substitution is not true. Since the separation of these parts is complicated, the whole of scatter signal is used in developed method although some errors will be inserted into error functions due to the second part of scatter signal. On the other hand, the speed of lower frequency lamb waves is lower than higher frequency waves. Therefore, using lower frequency lamb waves result in fewer reflections of damage scatters from structure boundaries in the scatter signal. Hence, using low frequency lamb wave leads to inserting less error into error functions and result in more accurate damage identification image, as can be distinguish from Fig. 10(b) and Fig. 12.

### 5.3 Crack detection using developed algorithm

In order to validate the efficiency of presented method in highlighting small damages, a through thickness crack was introduced into the plate as shown in Fig. 13. Experimental process starts with collecting the response of the intact and damaged plate at 150 KHz. The scattered or difference response of those paths are specified and the RMS values of each scatter signal is defined. Six error functions are determined and subsequently by Eq. (10) the resultant error function is specified and displayed in Fig. 14.

The probability values were normalized. As shown in Fig. 14, the location of defined crack can be identified from the resultant error function that shows the efficiency of developed technique to identify small damage in plates. However, since the introduced crack is smaller than Hole, more errors due to noise was inserted to error functions and as a result diagnostic image defined for crack (Fig. 14) is not as accurate as results defined for Hole (Fig. 11).

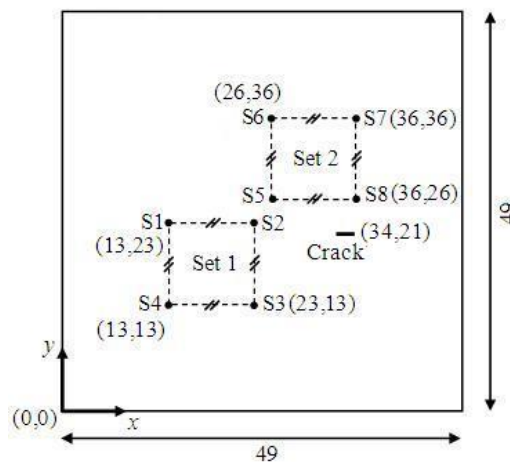


Fig. 13 Schematic diagram of aluminum plate with a through-thickness crack (dimensions in cm)

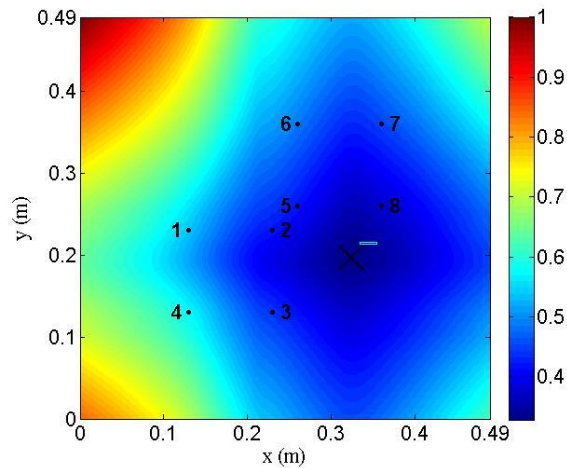


Fig. 14 The Probability of the presence of through-thickness crack (150 KHz) defined by 6 error functions using experimental signals

#### 4. Conclusions

A probabilistic damage diagnostic algorithm based on error functions using lamb wave signals was evaluated through both finite element analysis and experimental studies. For a certain sensing paths, the changes in signals before and after the introduction of damage were measured and by taking root mean square of these changes, the energy of the scatter signals till different times were obtained. According to the energy of the scatter signals for each pair of parallel paths, an error function was introduced. The resultant error function leads to the final estimation of the probability of the presence of damage.

An aluminum plate with a hole were examined using finite element analysis and also experimentally. In order to affirm the sufficiency of the presented algorithm, different central frequencies (150, 200, 250 KHz) were used in experiment. The central location of identified Hole at different central frequencies agreed well with the actual situation. However, it was shown that using lower frequency lamb waves result in fewer reflections of damage scatters from structure boundaries in the scatter signal. Hence, using low frequency lamb wave leads to inserting less error into error functions and result in more accurate damage identification image.

The efficiency of presented method in highlighting small damages was also shown by defining a through thickness crack in aluminum plate. Based on experimental results it was demonstrated that even if the response of the intact and damaged structure in one or some of paths defined incorrectly due to different sources of error which are inevitable, still the total result will show the location of damage clearly.

The identification results from both simulation and experiments demonstrated that this probabilistic-based algorithm without direct interpretation of overlaid and dispersed Lamb wave components, has the good potential to locate damage in the structures.

## Acknowledgments

This work was supported by the National Natural Science Foundation of China (51475067, 11172053 and 91016024) and the New Century Excellent Talents in University (NCET-11-0055) and the Fundamental Research Funds for the Central Universities (DUT12LK33 and DUT13ZD(G)06).

## References

- Coverley, P.T. and Staszewski, W.J. (2003), "Impact damage location in composite structures using optimized sensor triangulation procedure", *Smart Mater. Struct.*, **12**(5), 795-803.
- Hu, N., Shimomukai, T., Fukunaga, H. and Su, Z. (2008), "Damage identification of metallic structures using A0 mode of lamb waves", *Struct. Health Monit.*, **7**(3), 271-285.
- Ihn, J.B. and Chang, F.K. (2004), "Detection and monitoring of hidden fatigue crack growth using a built-in piezoelectric sensor/actuator network: I. Diagnostics", *Smart Mater. Struct.*, **13**(3), 609-620.
- Ihn, J.B. and Chang, F.K. (2008), "Pitch-catch active sensing methods in structural health monitoring for aircraft structures", *Struct. Health Monit.*, **7**(1), 5-19.
- Kundu, T., Das, S. and Jata, K.V. (2009), "Health monitoring of a thermal protection system using lamb waves", *Struct. Health Monit.*, **8**(1), 29-45.
- Lin, B. and Giurgiutiu, V. (2006), "Modeling and testing of PZT and PVDF piezoelectric wafer active sensors", *Smart Mater. Struct.*, **15**(4), 1085-1093.
- Ling, H.Y., Lau, K.T., Cheng, L. and Jin, W. (2005), "Fibre optic sensors for delamination identification in composite beams using a genetic algorithm", *Smart Mater. Struct.*, **14**(1), 287-295.
- Park, S., Yun, C.B., Roh, Y. and Lee, J.J. (2006), "PZT-based active damage detection techniques for steel bridge components", *Smart Mater. Struct.*, **15**(4), 957-966.
- Sohn, H. and Lee, S.J. (2010), "Lamb wave tuning curve calibration for surface-bonded piezoelectric transducers", *Smart Mater. Struct.*, **19**(1), 015007.
- Sohn, H., Park, G., Wait, J.R., Limback, N.P. and Farrar, C.R. (2004), "Wavelet-based active sensing for delamination detection in composite structures", *Smart Mater. Struct.*, **13**(1), 153-160.
- Su, Z. and Ye, L. (2004), "Lamb wave-based quantitative identification of delamination in CF/EP composite structures using artificial neural algorithm", *Compos. Struct.*, **66**(1-4), 627-637.
- Su, Z., Ye, L. and Lu, Y. (2006), "Guided lamb waves for identification of damage in composite structures: A review", *J. Sound Vib.*, **295**(3-5), 753-780.
- Wang, C.H., Rose, J.T. and Chang, F.K. (2003), "A computerized time-reversal method for structural health monitoring", *Proceedings of the SPIE Conference on Smart Structures/NDE*, San Diego.
- Wang, C.H., Rose, J.T. and Chang, F.K. (2004), "A synthetic time-reversal imaging method for structural health monitoring", *Smart Mater. Struct.*, **13**(2), 413-423.
- Wang, D., Ye, L., Su, Z., Lu, Y., Li, F. and Meng, G. (2010), "Probabilistic damage identification based on correlation analysis using guided wave signals in aluminum plates", *Struct. Health Monit.*, **9**(2), 133-144.
- Wang, L. and Yuan, F.G. (2005), "Damage identification in a composite plate using prestack reverse-time migration technique", *Struct. Health Monit.*, **4**(3), 195-211.
- Worden, K. and Lane, A.J. (2001), "Damage identification using support vector machines", *Smart Mater. Struct.*, **10**(3), 540-547.
- Wu, Z. and Chang, F.K. (2009), "Damage detection for composite laminate plates with a distributed hybrid PZT/FBG sensor network", *J. Intel. Mat. Syst. Str.*, **20**(9), 1069-1077.
- Ye, L., Su, Z., Yang, C., He, Z. and Wang, X. (2006), "Hierarchical development of training database for artificial neural network-based damage identification", *Compos. Struct.*, **76**(3), 224-233.
- Zhou, C., Su, Z. and Cheng, L. (2011), "Probability-based diagnostic imaging using hybrid features

extracted from ultrasonic Lamb wave signals”, *Smart Mater. Struct.*, **20**(12), 125005.

CY